



Synthesis and characterization of as-grown doped polymerized (PMMA-PVA)/ZnO NPs hybrid thin films

A. M. Alsaad¹ · Abdul Raouf Al Dairy² · A. A. Ahmad¹ · Ayah S. Al-anbar² · Qais M. Al-Bataineh¹

Received: 13 October 2020 / Revised: 20 January 2021 / Accepted: 23 February 2021 /
Published online: 5 March 2021

© The Author(s), under exclusive licence to Springer-Verlag GmbH Germany, part of Springer Nature 2021

Abstract

We report the optical, lattice dynamical, and thermal characterization of the poly-methyl-meth-acrylate (PMMA) and poly-vinyl-alcohol (PVA) doped with (wt% = 2%, 4%, 8%, and 16%) of zinc oxide nanoparticles (ZnO NPs) deposited on glass substrate. The optical properties of as-prepared (PMMA-PVA)/ZnO NPs hybrid thin films such as transmittance ($T\%$), reflectance ($R\%$), absorption coefficient (α), optical constants (n and k), and optical dielectric functions (ϵ_1 and ϵ_2) are deduced using the experimental transmittance and reflectance spectra. Furthermore, a combination of classical models such as Tauc, Urbach, Spitzer–Fan, and Drude models are utilized to calculate the optical and optoelectronic parameters and the band gap of the as-grown nanocomposite thin films. Calculated refractive indices (n) of pure PMMA-PVA polymeric thin films are found to lie in the range (1.5–1.85). We found the optical band gap of PMMA-PVA thin film to be 4.101 eV. Introducing ZnO NPs into PMMA-PVA polymeric matrix leads to a noticeable decrease of the optical band gap. Furthermore, Fourier transform infrared spectroscopy (FTIR) transmittance spectra are measured and interpreted in the spectral range (500–4000 cm^{-1}) to identify the vibrational bands associated with the formation, rotation, and twisting of different bonds. Thermogravimetric analysis (TGA) is performed to test the thermal stability of as-grown thin films. We found that as-grown thin films are thermally stable below 110 °C. Therefore, realistic, scaled and practical devices based on doped polymerized films can be fabricated. Tuning optical, chemical, and thermal properties is of prime importance for the fabrication of state-of-the-art high-tech devices.

Keywords Hybrid thin films · Poly-methyl-meth-acrylate (PMMA) · Poly-vinyl-alcohol (PVA) · Zinc oxide nanoparticles (ZnO NPs) · Optical properties · Dip coating technique

✉ A. M. Alsaad
alsaad11@just.edu.jo; amalsaad@unomaha.edu

Extended author information available on the last page of the article

Introduction

Organic–inorganic nanocomposite thin films have increasingly gained interest owing to their outstanding properties. Doped polymeric films constitute an important class of nanocomposite materials with nanofillers are homogeneously diffused in the polymer matrix [1–3]. Such blends are usually prepared by mechanical mixing of a polymer with metal nanoparticles via melt mixing, in situ polymerization of a monomer in the presence of metal nanoparticles or in situ reduction of metal salts or complexes in a polymer matrix [4]. Nanocomposites often exhibit physical and chemical properties that are radically different from conventional microcomposites [5].

Hybrid thin films have been widely synthesized by different techniques such as emulsion polymerization [6, 7], microemulsion polymerization [8], solution polymerization [9], sol–gel method [10], sputtering, chemical vapor deposition (CVD), ion beam evaporation and pulse laser deposition [11]. However, the sol–gel technique has been increasingly conducted by researchers in the last few years to fabricate zinc oxide thin films due to the low cost of organic precursor used, simple tools used, low substrate temperature, and the feasibility of producing high-quality films [12].

The mechanical and thermal properties of the nanocomposites are improved upon introducing suitable nanoparticles. Doped polymeric thin films have been widely used for chromatographic separations, biochemistries, bioengineering, dental materials, and prosthetic replacement operations [13–15]. Our motivation to conduct this work stems from the fact that several inorganic nanoparticles have been introduced to improve the mechanical and thermal properties of PMMA [16]. In addition, PMMA is an important member in the family of polyacrylic and methacrylic esters [16]. PMMA has acquired unlimited interest and great features owing to its individual properties such as its exceptional optical clarity, good weatherability, and high strength, and excellent dimensional stability, lower optical absorption due to its high transparency in the visible region, low refractive index, hardness, thermal capacity, electrical performance, good mechanical properties, and simple synthesis [17].

Poly(vinyl alcohol) (PVA) is a polymer that has been studied intensively because of its good film forming and physical properties, high hydrophilicity, processability, biocompatibility, and good chemical resistance [18]. The properties of PVA can be improved or modified by adding inorganic functional materials [19]. PMMA-PVA nanocomposite has attracted much interest for scaled industrial applications [20]. This is mainly due to its lightweight, good mechanical strength, and outstanding optical properties [21].

ZnO semiconductors have been widely investigated [22]. ZnO nanoparticles have attracted global attraction due to its outstanding physical properties [23, 24], its chemical stability, catalytic activity, antibacterial property, less toxicity, wide band gap (3.37 eV), large exciton binding energy around (60 meV), high refractive index, and ultraviolet absorption [25–29]. It has been widely used in preparing solar cells [30], gas sensors [31, 32], varistors catalysts [33–35], electrical

and optical devices [36–38], and electrostatic dissipative coatings [39]. The ZnO nanoparticles can be synthesized by homogeneous precipitation [40], mechanical milling [41], spray pyrolysis [42], and homogeneous precipitation [43]. The ZnO NPs have been added to several polymers, such as PMMA, PS, PVA, PVC, and PC, to enhance their physical and chemical properties [44–47].

The aim of this study is threefold. First, we synthesize high-quality (PMMA-PVA)/ZnO NPs hybrid thin films of sizes appropriate for a diversity of applications. Secondly, we characterize the as-grown films optically by measuring their transmittance ($T\%$), reflectance ($R\%$), index of refraction (n), extinction coefficient (k), Urbach energy (E_U), and optical band-gap energies (E_U). Thirdly, chemical, vibrational, and thermal properties are investigated and interpreted by conducting and analyzing FTIR and TGA measurements.

Experimental details

Preparation of zinc oxide nanoparticles (ZnO NPs)

To prepare the ZnO nanoparticles, 2.18 g of zinc acetate dehydrate [$\text{Zn}(\text{CH}_3\text{CO}_2)_2 \cdot 2\text{H}_2\text{O}$] is dissolved in 40 mL of absolute ethanol in a beaker (Sol.1) using magnetic stirrer. In a different beaker (Sol.2), 0.4 g of NaOH was added to 40 mL of absolute ethanol. Both beakers are subsequently placed on a magnetic stirrer for twenty minutes. Once the mixing process is over, Sol.1 is placed in a water bath at a temperature of 70°C for 3 h. Next, the content of Sol.2 is dropped into Sol.1. and the ZnO NPs are separated from the ethanol by centrifugation. To obtain ZnO NPs in the powder form, the resulting solution is placed in a furnace at 60°C to 70°C for 24 h [48].

(PMMA-PVA) doped by ZnO NPs thin films

PMMA-PVA and PMMA-PVA incorporated with ZnO NPs composites in the form of thin films are synthesized. A stock solution of PMMA-PVA in *Chloroform* (CHCl_3) was prepared by dissolving 1 g of PMMA and 1 g of PVA in 200 mL *Chloroform*. Magnetic stirring was performed for about 24 h. Pre-calculated amount of metal oxides nanoparticles (2%, 4%, 8%, and 16% of ZnO NPs) were added directly into a flask connect of PMMA-PVA solutions to produce metal oxides network in PMMA-PVA matrix. The entire solutions were stirred until the metal oxides nanoparticles have completely dissolved and dispensed. Smooth films were obtained by dipping the glass substrate in the solution for 2 h to get a film of 500 nm thickness. The films were dried in an oven for 15 min at 70 °C to evaporate the solvent and organic residues.

Results and discussion

UV–Vis spectroscopy

The spectrophotometer with a total internal reflectance sphere is used to investigate the optical properties of (PMMA-PVA)/ZnO NPs nanocomposite thin films at various concentrations of ZnO NPs. Light is incident from the ambient (air) on thin films that is transmitted to the substrate and emerged from the air on the other side of thin-film samples. Figure 1 shows the transmittance spectra of (PMMA-PVA)/ZnO NPs nanocomposite thin films at various concentrations of ZnO NPs deposited by dip coating technique. We found that undoped (PMMA-PVA) thin film exhibits high transmittance of about 91.6% at $\lambda=550$ nm in the visible region. The addition of 2% and 4% ZnO NPs to the polymer solution results in a decrease of transmittance to 88.38% and 87.73%, respectively. Increasing ZnO NPs in the polymer matrix to 8% causes a further decrease of the transmittance to 86.5%. A drastic decrease of transmittance to 79.4% as ZnO NPs concentration is increased to 16% in the polymer matrix. Additionally, an abrupt decrease of transmittance in the UV region (0–400) nm is detected indicating strong electronic transitions occur within the band gap that is considered as high-absorption region.

Figure 2 shows the reflectance of (PMMA-PVA)/ZnO NPs nanocomposite thin films at various concentrations of ZnO NPs. Obviously, as the ZnO NPs content in the polymeric film is increased, reflectance increases. We found that undoped (PMMA-PVA) thin film has low reflectance of about 4.6% in the visible region. Insertion of 2% and 4% ZnO NPs into the polymer solution increases reflectance to 6.2% and 7.3% in the visible spectrum region. We noticed that injection of 8% and 16% ZnO NPs into the polymeric matrix raises the reflectance to 7.6% and

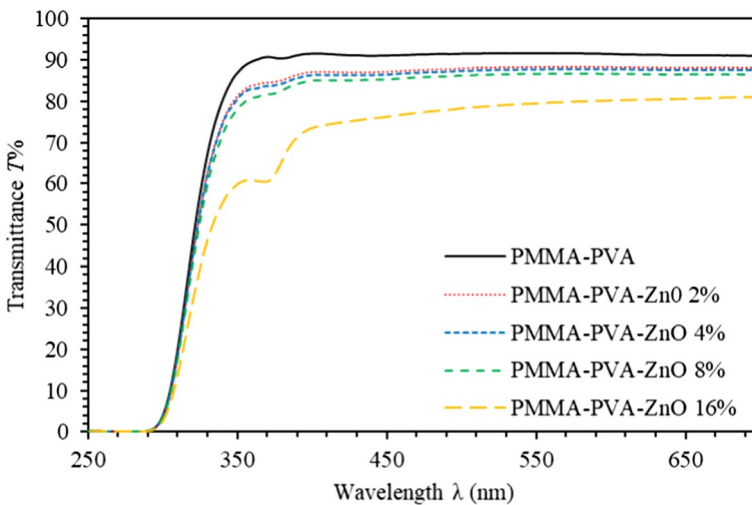


Fig. 1 Transmittance spectra of (PMMA-PVA)/ZnO NPs nanocomposite thin films at various concentrations of ZnO NPs deposited by dip coating technique

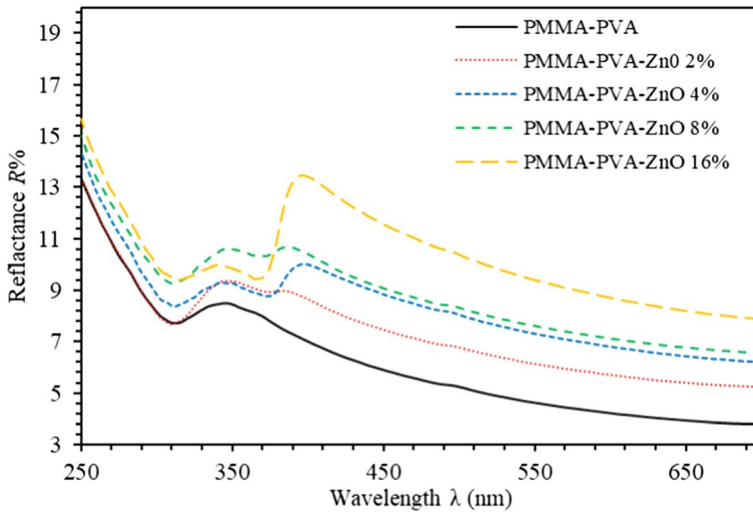


Fig. 2 Reflectance spectra of (PMMA-PVA)/ZnO NPs nanocomposite thin films at various concentrations of ZnO NPs deposited by dip coating technique

9.4%, respectively. Our results are promising in the sense that a gradual increase of reflectance as we add more concentration of ZnO NPs indicates that optical properties of (PMMA-PVA)-ZnO NPs nanocomposite thin films could be modified to produce highly reflective materials. It could be used for the fabrication of products like reflective tape, reflective ink, reflective marking paint, reflective cloth, reflective leather, reflective ribbon, and reflective safety silk fabric. Using such high reflective coatings could yield reflective materials that have several hundred times chromatic effects than other non-reflective materials. Reflective materials have been widely used in various warning signs, lifesaving marks, textile products, advertising, and other fields.

Optical absorption results provide deeper insight into understanding the optical band gap (E_g), the nature of electronic transitions between the valance bands and the conduction bands in the materials, Urbach energy (E_U), Steepness parameter (σ) and electron–phonon interaction energy (E_{e-p}). The study of absorption coefficient spectra of a polymer, hybrid material and semiconducting thin films is usually conducted in two steps according to the spectral region investigated. Mainly, in the high-energy part of the spectrum, the absorption coefficient spectra are characterized by the electronic states involved in the transition, and the lower part is categorized by atomic vibrations. The study of atomic vibrations provides a direct way of obtaining band-gap energy and the details of the band structure [49–51]. Figure 3 shows the absorption coefficient (α) of (PMMA-PVA)/ZnO NPs nanocomposite thin films at various concentrations of ZnO NPs. Our results indicate that undoped (PMMA-PVA) thin film exhibits vanishingly small α value found to be about 0.0116 in the UV region that attenuates sharply to 0.00017 in the visible region. Addition of 2%, 4% and 8% ZnO NPs to the polymer solution, results in α values of 0.00025, 0.00026, 0.00029 in the visible region, respectively. Highly doped (PMMA-PVA)-ZNO NPs

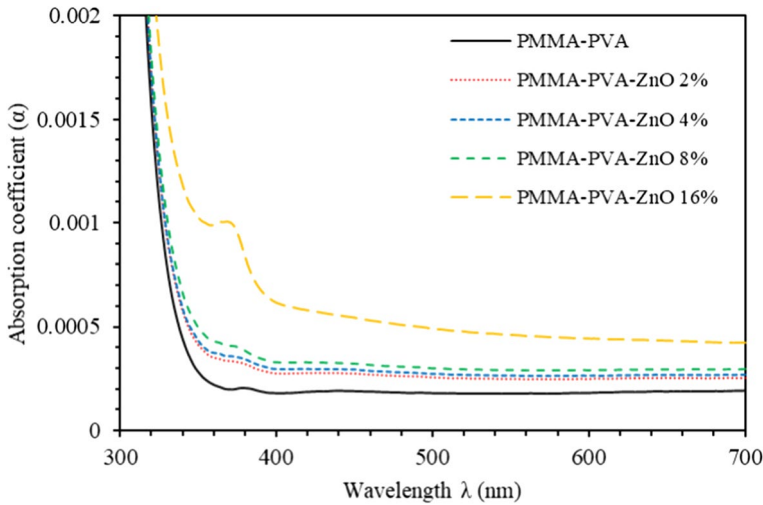


Fig. 3 Absorption coefficient (α) of (PMMA-PVA)/ZnO NPs nanocomposite thin films at various concentrations of ZnO NPs deposited by dip coating technique

nanocomposite thin films demonstrate large α coefficients. In particular, α increases to 0.00046 as ZnO NPs concentration increases to 16% in the polymer matrix. The α parameter attains approximately fixed value in the visible spectrum region as the content of ZnO NPs increases. Richly doped (PMMA-PVA)-ZnO NPs nanocomposite thin films act like as light filter for the entire range of visible spectrum.

Index of refraction n plays an important role in selecting the materials for specific optical applications. It can be calculated as,

$$n = \left(\frac{1+R}{1-R} \right) + \sqrt{\frac{4R}{(1-R)^2} - k^2} \quad (1)$$

The refractive index (n) as a function of the wavelength of incident light is shown in Fig. 4. In a high-absorption region ($\lambda < 400$ nm), the incident photon frequency resonates with the plasma frequency. In the spectral region, $\lambda \geq 400$ nm, the refractive index decreases abruptly with wavelength and exhibits normal dispersion. In the high-wavelength region, it saturates and attains approximately constant value. We found that n of (PMMA-PVA) thin film exhibits values ranging between 1.48 and 1.55 as the wavelength of incident light decreases from 700 to 400 nm. Insertion of 2% and 4% of ZnO NPs into polymeric matrix leads to a significant increase in the values of n to 1.65 and 1.73, respectively. Injection of 8% and 16% of ZnO NPs into the polymer solution leads to a further increase of n values to 2.2 and 2.3, respectively. The significant increase in the values of n as the concentration of ZnO NPs increases could be attributed to the condensation of smaller ions into larger clusters as the NPs dispersed uniformly into the polymeric thin films [52]. As a result, (PMMA-PVA)/ZnO NPs nanocomposite thin films could be used for typical tasks such as photovoltaics, medical technology, semiconductor, flat-panel display, and

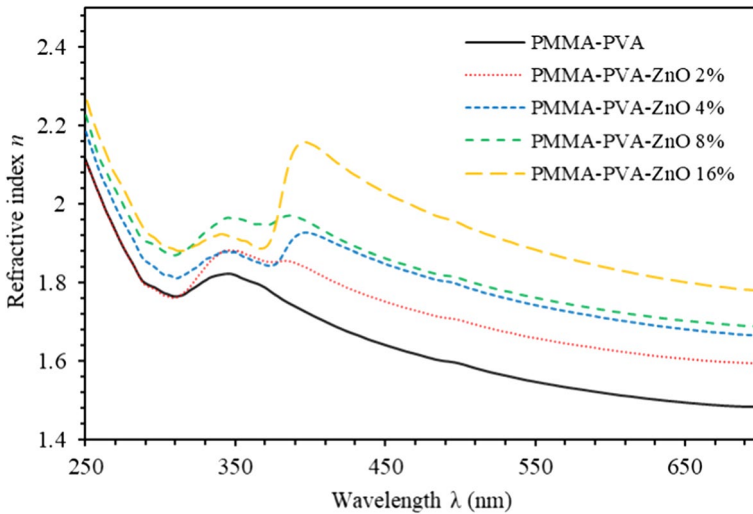


Fig. 4 Refractive index (*n*) of (PMMA-PVA)/ZnO NPs nanocomposite thin films at various concentrations of ZnO NPs deposited by dip coating technique

organic light-emitting diodes (OLED) production. Moreover, they may be employed in glass and optical industries.

Extinction coefficient (*k*) has an important role in the determination of a few optical parameters, chiefly those related to the absorption of light waves in the medium. *k* value measures the fraction of light lost due to the scattering and absorption per unit distance of the infiltration medium. It can be expressed (2) as,

$$k = \frac{\alpha\lambda}{4\pi} \tag{2}$$

where α is the absorption coefficient given by $\alpha = (1/d) \ln(1/T)$, with *d* being the average thickness of films measured to be 500 nm. Figure 5 displays *k* values of (PMMA-PVA)/ZnO NPs nanocomposite thin films at various concentrations of ZnO NPs. We insert 2%, 4%, 8% and 16% of ZnO NPs into the polymeric thin films. We observed a significant gradual increase of the value of *k*. In particular, we found that injection of 16% ZnO NPs increases α significantly indicating that high amount of light energy is being lost due to scattering and absorption in (PMMA-PVA)/ZnO NPs doped with a high concentration of ZnO NPs.

Dielectric parameter is closely related to the electronic band structure and sensitive to the density of states in the forbidden gap of a material. The complex dielectric function ($\epsilon = \epsilon' + i\epsilon''$) is related to complex refractive index (*N*) by the equation: $\epsilon = N^2$ [49]. The calculation of dielectric function is achieved practically in terms of optical constants *n* and *k*. The two parameters are related to optical dielectric constant (ϵ') and optical dielectric loss (ϵ'') by $\epsilon' = n^2 + k^2$ and $\epsilon'' = 2nk$ [50]. Figures 6 and 7 show the dielectric functions (ϵ' and ϵ'') of (PMMA-PVA)/ZnO NPs nanocomposite thin films as functions of incident wavelength for various concentrations of ZnO NPs. The index of refraction and extinction coefficient spectra exhibit similar trends since

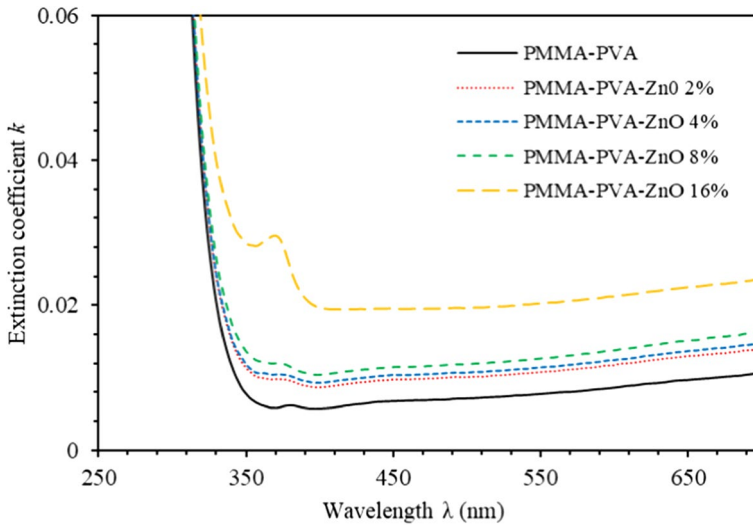


Fig. 5 The extinction coefficient (k) of (PMMA-PVA)/ZnO NPs nanocomposite thin films at various concentrations of ZnO NPs deposited by dip coating technique

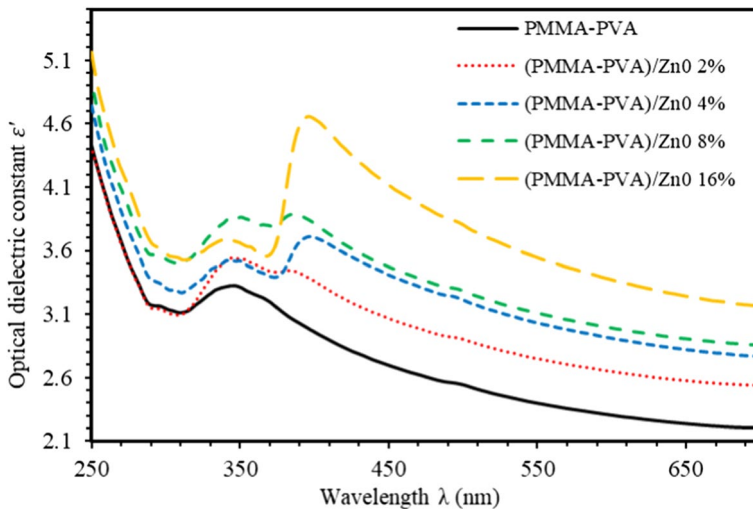


Fig. 6 Optical dielectric constant (ϵ') spectra of (PMMA-PVA)/ZnO NPs nanocomposite thin films at various concentrations of ZnO NPs deposited by dip coating technique

the four optical constants are related to each other via $\epsilon' = n^2 + k^2$ where $n \gg k$, while $\epsilon'' = 2nk$ where k diminishes this product value. It is also observed that the values of the real part are comparatively higher than those of an imaginary one ($\epsilon' \gg \epsilon''$). Subsequently, the low ϵ'' values account for the less dissipation of energy. In general, addition

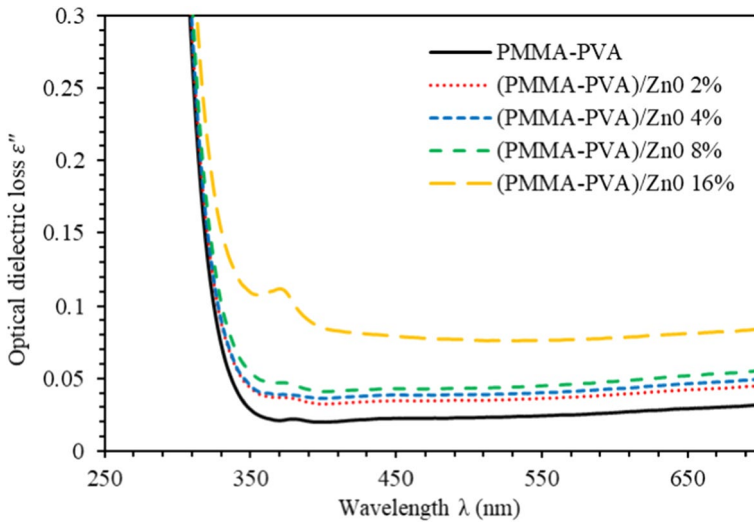


Fig. 7 Optical dielectric constant (ϵ'') spectra of (PMMA-PVA)/ZnO NPs nanocomposite thin films at various concentrations of ZnO NPs deposited by dip coating technique

of ZnO NPs to the composite polymer leads to an increase of the dielectric functions (ϵ' and ϵ'') in the visible spectrum region.

Tauc plot of undoped and doped polymeric thin films obtained by plotting the incident photon energy ($h\nu$) versus $(\alpha h\nu)^2$. The plots are utilized to calculate the optical energy band gap E_g according to Tauc’s formula [51], $(\alpha h\nu) = B(h\nu - E_g)^m$, where B is a band tailing parameter, E_g is the optical band gap, $h\nu$ is photon energy, and m is the power factor that determines the type of transition. It exhibits the values of 1/2, 3/2, 2, and 3 for allowed direct, forbidden direct, allowed indirect and forbidden indirect transitions, respectively. Figure 8 shows the Tauc plot of doped and undoped (PMMA-PVA)/ZnO NPs nanocomposite thin films obtained by plotting photon energy ($h\nu$) versus $(\alpha h\nu)^2$. The main goal of this plot is to estimate band-gap energy E_g . The E_g of undoped (PMMA-PVA) thin film is found to be 4.069 eV. Addition of 2%, 4%, 8% and 16% ZnO NPs to the polymer solution results in a gradual slight decrease of E_g to 4.041 eV, 4.016 eV, 3.98 eV, and 3.96 eV, respectively, as illustrated in Fig. 8. The manipulation of the band gap of the investigated doped polymeric thin films is anticipated to play a crucial role in organic electronics and the development of technological applications such as sensors, electrochromic devices, organic light-emitting diodes (OLEDs), and field-effect transistors (FETs).

In order to determine the width of the defect states formed inside thin film’s band gap, we employ the Urbach model. The advantage of using this model is its validity and feasibility to account for the shifts that can arise between the extended state of valance band maximum and localized state of the condition band minimum, Urbach empirical formula can be written as,

$$\alpha = \alpha_0 \exp (h\nu/E_U) \tag{3}$$

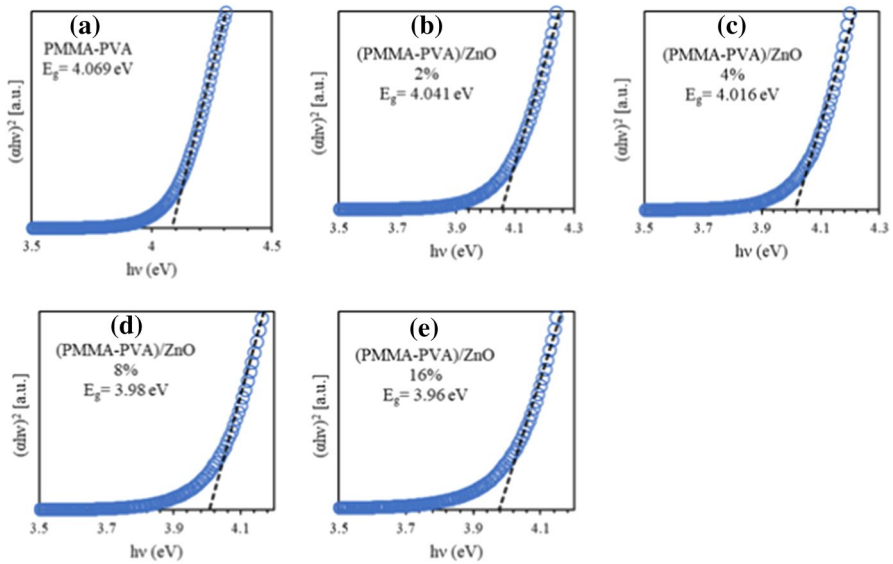


Fig. 8 The Tauc optical band-gap energy of the dip-coated (PMMA-PVA)/ZnO NPs nanocomposite thin films at various concentrations of ZnO NPs deposited by dip coating technique

where α_0 is a constant, $h\nu$ is the incident photon energy, and E_U is the band tail width (Urbach energy) of confined states in the optical band gap. Figure 9 shows Urbach energy E_U as a function of the incident photon energy of (PMMA-PVA)/ZnO NPs nanocomposites for different ZnO NPs concentrations. The width of the localized states of Urbach energy can be estimated from the slope of $\ln(\alpha)$ in the linear region.

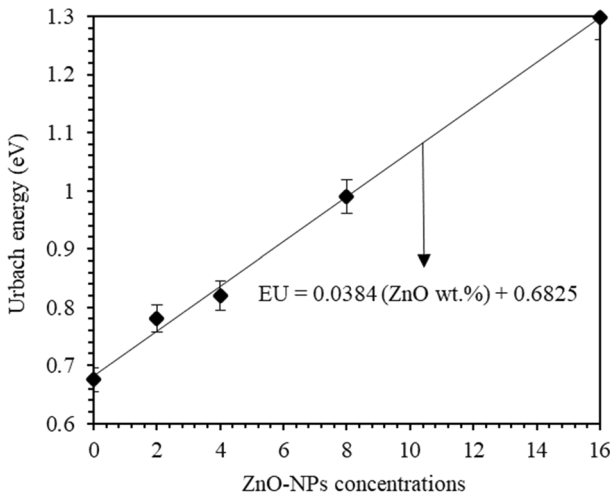


Fig. 9 Variation of Urbach energy E_U of the (PMMA-PVA)/ZnO NPs nanocomposites as a function of different concentration of ZnO NPs

E_U is simply the inverse of this slope. As can be clearly seen from Fig. 9, E_U increases linearly for the high concentration of ZnO NPs. The higher value of E_U confirms low crystallinity and strong disorder in the 16% ZnO NPs doped nanocomposite polymeric thin films.

Figure 10 shows the converse relationship between E_U and E_g . Obviously, E_g increases as E_U decreases when ZnO NPs concentration in the polymeric matrix is increased. This result can be interpreted as follows: as E_U increases, the disorder and defect states within the film texture appear to become pronounced and thus it leads to a significant increment of the band tail width in the band structure of thin films. Consequently, a decrease in the band-gap energy of the hybrid films is observed.

Optoelectronic parameters

Fundamentally, electronic, ionic, dipolar, and space charge polarization contribute to the dielectric function of thin films. The space charge contribution depends on the purity and the aptness of the glass substrate. Customarily, the influence of the space charge contribution is intensely noticeable in the low-frequency region. In the lower-frequency region known as a normal dispersion region, the refractive index n equal the dielectric constant ϵ' and can be related to the density of states (ratio of free carrier to the effective mass) N/m^* and the high-frequency dielectric constant ϵ_∞ as expressed by Spitzer–Fan [52, 53],

$$n^2 = \epsilon' = \epsilon_\infty - \frac{1}{4\pi^2\epsilon_0} \left(\frac{e^2}{c^2} \right) \left(\frac{N_c}{m^*} \right) \lambda^2 \tag{4}$$

where e is the electronic charge, c is the light speed, N_c is the charge carrier density and m^* is the effective mass of the carrier. Plotting n^2 versus λ^2 yields a

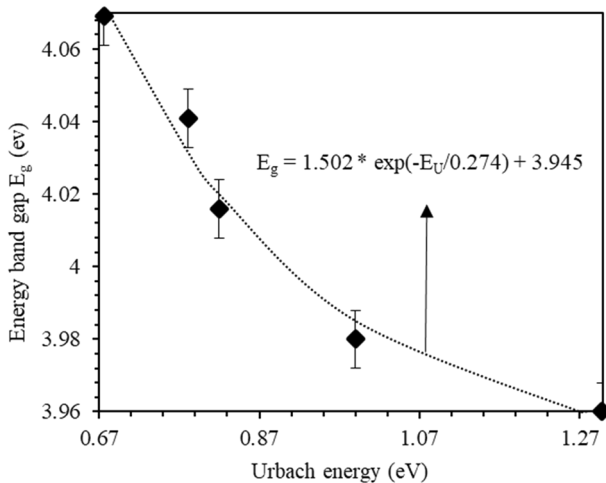


Fig. 10 Relationship of the optical energy gap and the Urbach’s energy of the (PMMA-PVA)/ZnO NPs nanocomposites at different concentrations of ZnO NPs

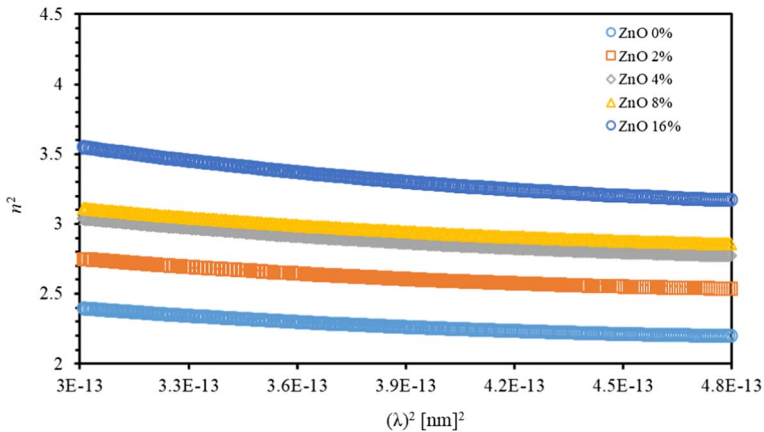


Fig. 11 The variation of the real part of the dielectric constant ($n^2 = \epsilon'$) with the square of the photon wavelength (λ^2) for (PMMA-PVA)/ZnO NPs nanocomposite thin films for various ZnO NPs concentrations deposited by dip coating technique

Table 1 Estimation of some essential optical parameters of the (PMMA-PVA)/ZnO NPs nanocomposite thin films for various ZnO NPs concentrations

Parameter	ZnO 0%	ZnO 2%	ZnO 4%	ZnO 8%	ZnO 16%
Density of states, $N_c/m^* * 10^{+57} (\text{m}^{-3} \text{kg}^{-1})$	1.066	1.211	1.589	1.520	2.404
Charge carrier density, $N_c * 10^{+27} (\text{m}^{-3})$	4.273	4.852	6.372	6.090	9.635
High-frequency dielectric constant, ϵ_∞	2.623	3.012	3.388	3.445	4.093
Relaxation time, $\tau * 10^{-14} (\text{s})$	2.493	2.439	2.943	2.463	2.429
Optical mobility, $\mu_{opt} * 10^{-3}$	9.951	9.739	11.749	9.833	9.697
Optical resistivity, $\rho_{opt} * 10^{-6}$	1.470	1.323	0.835	1.043	0.669

straight line in the long-wavelength region. The ratio N/m^* can be determined from the slope of the linear part, while ϵ_∞ is usually determined by extending the linear part of this curve to $\lambda^2 = 0$. Figure 11 shows the dispersion nature of the index of refraction of (PMMA-PVA)/ZnO NPs nanocomposite thin films. The estimated values of both ϵ_∞ and N_c/m^* are listed in Table 1. The value of ϵ_∞ of (PMMA-PVA) thin films is found to be 2.623. Addition of 2%, 4%, 8%, and 16% of ZnO NPs to PMMA-PVA polymeric thin films increases ϵ_∞ to 3.012, 3.388, 3.445, and 4.093. Materials with high dielectric constant could be used for a variety of applications ranging from typical insulators in electrical and micro-electronic encapsulation to appliances where dielectric functions are utilized for active device designs such as rectifiers, transducers, ordinary and supercapacitors, and transformers. The obtained values of the dielectric constant at zero wavelength, ϵ_∞ are also found to be greater than the index of refraction, n , confirming the existence of the free charge carriers in (PMMA-PVA) and (PMMA-PVA)/

ZnO NPs nanocomposite thin films that intensely contribute to the polarization process [54, 55]. As a result, the value of the charge carrier’s density increases from $4.273 \times 10^{+27}$ to $9.635 \times 10^{+27}$ atoms/m³ as the ZnO NPs concentration added to (PMMA-PVA)/ZnO NPs nanocomposite thin films increase from 0 to 16%.

The imaginary part of the dielectric function (ϵ'') versus the wavelength of the incident photon is analyzed to determine the relaxation time (τ), optical mobility (μ_{opt}) and optical resistivity (ρ_{opt}) using Drude free electron model [52],

$$\epsilon'' = \frac{1}{4\pi^3 \epsilon_0} \left(\frac{e^2}{c^3} \right) \left(\frac{N_c}{m^*} \right) \left(\frac{1}{\tau} \right) \lambda^3 \tag{5}$$

Figure 12 shows the variation of the imaginary part of the dielectric constant (ϵ'') versus λ^3 for (PMMA-PVA)-ZnO NPs nanocomposite thin films at various concentrations of ZnO NPs. The relaxation time τ is determined from the slope of the plot of ϵ'' against λ^3 and from the value of N_c/m^* and taking $m^* = 0.44m_e$ [56]. From the determination of τ , the optical mobility (μ_{opt}), as well as the optical resistivity (ρ_{opt}) of the films, can be calculated as [52],

$$\mu_{opt} = \frac{e\tau}{m^*} \tag{6}$$

$$\rho_{opt} = \frac{1}{e\mu_{opt}N_c} \tag{7}$$

The calculated values of optical mobility (μ_{opt}) and optical resistivity (ρ_{opt}) are listed in Table 1.

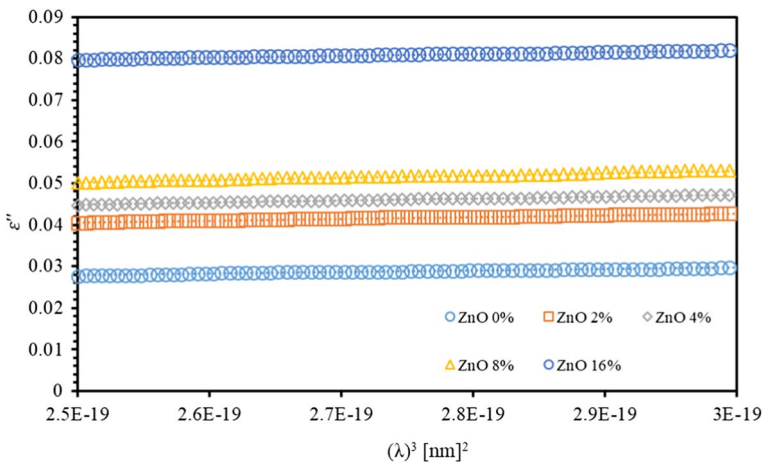


Fig. 12 The variation of the real part of the imaginary part of the dielectric constant (ϵ'') with the (λ^3) for (PMMA-PVA)/ZnO NPs nanocomposite thin films for various ZnO NPs concentrations deposited by dip coating technique

FTIR of (PMMA-PVA)/ZnO NPs nanocomposites thin films

The ability to tune the chemical and physical properties of surfaces using steady-state functionalization approaches is of vital significance for the progress in many industrial sectors, such as bio and chemical sensing [57], drug delivery [58], tissue engineering [59], solar cells [60], thin films batteries [61], and fabrication of semiconductor devices [62]. Recently, the prospect of engineering the chemical and physical properties of a surface by dispersing nanoparticles into thin polymer film has attracted significant consideration due to its easiness, strength, and tractability. Polymer films have attracted a great deal of research attempts [58, 59, 63, 64]. Thin polymer films can exhibit confinement-induced, peculiar physicochemical properties, such as changes in glass transition temperature [65], elastic moduli [66], and crystallization [67]. Characterizing the properties of such thin films is therefore of high significance both technologically and methodically.

The chemical behavior and structure of thin films are often characterized by infrared absorption spectroscopy [68–71] or other vibrational spectroscopy techniques such as surface-enhanced Raman Spectroscopy [72]. Thin-film IR spectroscopy is commonly performed using attenuated total reflectance Fourier transform infrared spectroscopy (FTIR) [71, 73, 74].

Fourier Transform Infrared spectroscopy (FTIR) is performed to investigate the vibrational bands of the nanocomposite. Figure 13 displays the FTIR spectra of (PMMA-PVA)/ZnO NPs nanocomposite thin films with 0%, 2%, 8%, and 16% of ZnO NPs as a function of the wavenumber in the range (500–4000 cm^{-1}). Figure 14 shows FTIR spectra of (PMMA-PVA)/ZnO NPs nanocomposites decomposed into three consecutive spectral ranges, mainly (a) (500–1500) cm^{-1} , (b) (1500–2500) cm^{-1} , and (c) (2500–4000) cm^{-1} . Our results indicate that PMMA-PVA polymer thin films exhibit vibrational band at 669 cm^{-1} and bands at 745.2 cm^{-1} and 926 cm^{-1} could be ascribed to the bending of C–O bond and C–H bond, respectively. Additionally, vibrational bands at 1214.5 cm^{-1} , 1494 cm^{-1} , and 1428.6 cm^{-1} could be attributed to the C–O bond stretching and O–H bond stretching, respectively. Likewise, vibrational band at 1725.08 cm^{-1} could be assigned to the stretching of C=O groups. Finally, the band at 3019 cm^{-1} could be attributed to C–H stretching of the Methylene group. In addition, we found that (PMMA-PVA)/ZnO NPs nanocomposite thin films exhibit vibrational bands at 1150.7 cm^{-1} that could be correlated with Zn–O bond. The observed increased bond intensity at 1725.08 cm^{-1} seems to be due to the presence of the (ester bond) stretching of PMMA-PVA. This could be explained by the fact that PMMA can coordinate with Zn^{2+} ions on the surface of the ZnO nanoparticles in good agreement with Gowri and et.al. within numerical accuracy [75]. The variations of the peak's intensities of the whole FTIR spectra of (PMMA-PVA)/ZnO NPs nanocomposite thin films may be interpreted in terms of the intermolecular bonding between the PMMA-PVA nanocomposites and ZnO NPs.

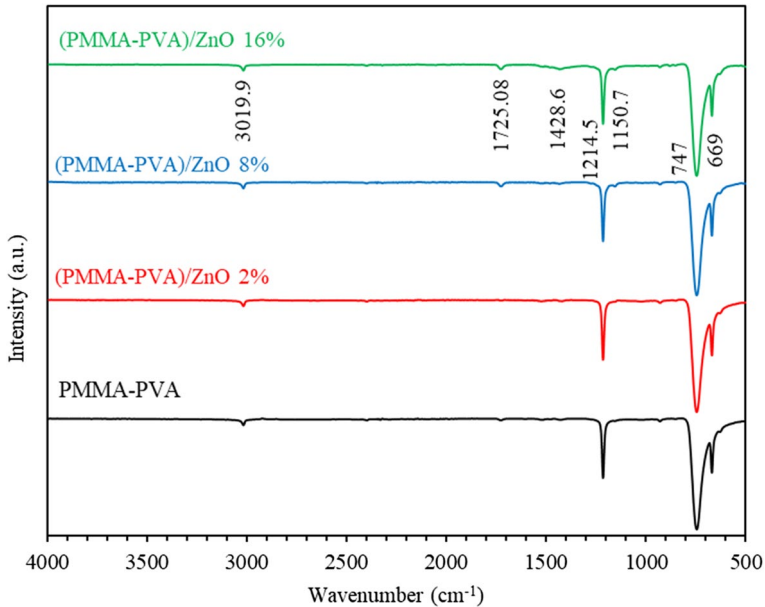


Fig. 13 The FTIR spectra of (PMMA-PVA)/ZnO NPs nanocomposite thin films as a function of wavenumber at different ZnO NPs concentrations

Thermogravimetric analysis (TGA) of (PMMA-PVA)/ZnO NPs thin films

The thermal stability of (PMMA-PVA)/ZnO NPs nanocomposite thin films is investigated by employing thermogravimetric analysis (TGA) at temperatures up to 400 °C as shown in Fig. 15. TGA thermograms of (PMMA-PVA)/ZnO NPs nanocomposites show considerable weight loss (WL) steps at different increasing temperatures, and heating rates based on adsorbed water, intermolecular/intramolecular bonding and chemical stability. The TGA profile of (PMMA-PVA)/ZnO NPs nanocomposites has two WL steps at 110 and 250 °C irrespective of the degree of incorporation of ZnO NPs in the PMMA-PVA polymeric thin films. The first WL and second WL were slightly shifted toward lower and higher temperatures demonstrating the effect of the change of intermolecular/intramolecular bonding. Similar to what our results on (PMMA-PVA)-SiO₂ NPs, the WL of (PMMA-PVA)/ZnO NPs nanocomposite thin films is found to be inversely proportional to the wt.% of ZnO NPs, indicating the strengthen of physicochemical bonding density by increasing the incorporation degree with ZnO NPs. Advantageously, (PMMA-PVA)/ZnO NPs nanocomposites materials are found to be thermally stable at temperatures below 110 °C at which most of the optical applications of the nanocomposite can be accomplished. Despite that the slight and negligible slope in TGA curve below 110 °C occurred due to water/solvent adsorption and can be tackled using proper techniques of water treatment, thermal stability of all investigated thin films has been confirmed.

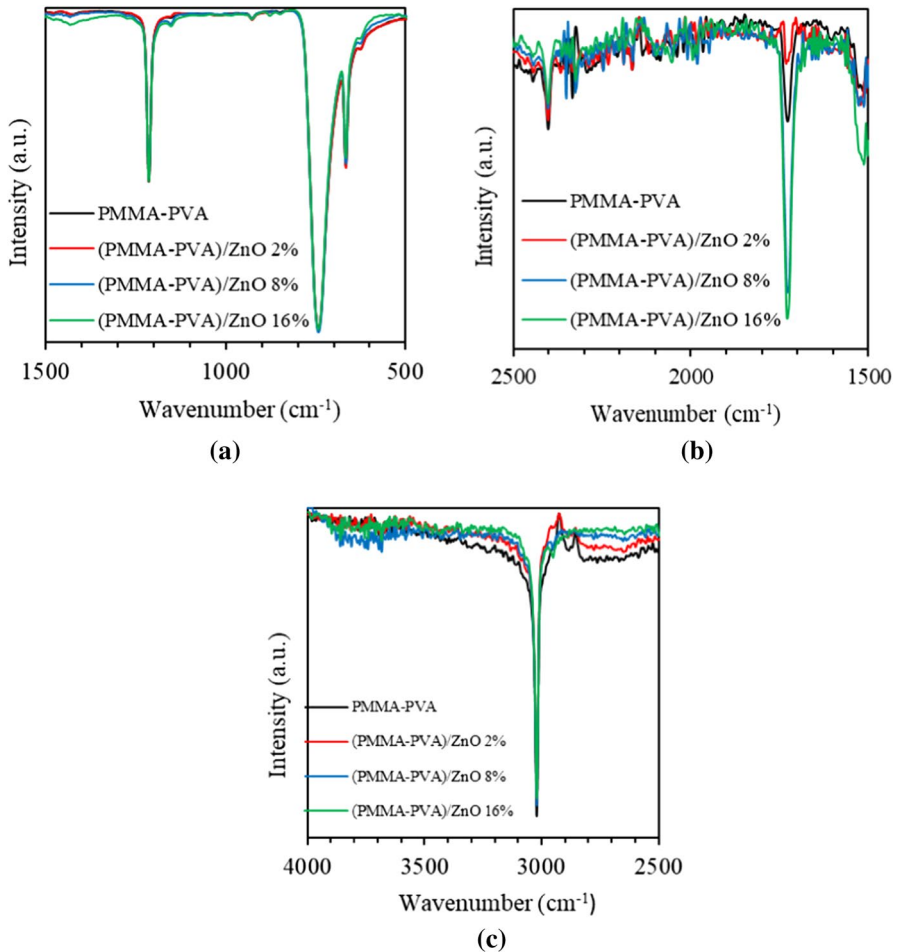


Fig. 14 The FTIR spectra of (PMMA-PVA)/ZnO NPs nanocomposite thin films as a function of wavenumber at different ZnO NPs concentrations decomposed into three consecutive spectral ranges: (a) (500–1500) cm⁻¹, (b) (1500–2500) cm⁻¹ and (c) (2500–4000) cm⁻¹

Scanning electron microscope (SEM)

The features of surface morphology of (PMMA-PVA)/ZnO NPs nanocomposites are examined using scanning electron microscopy (SEM). The SEM micrographs for different concentrations of ZnO NPs magnified at 20 μm magnification scale are shown in Fig. 16. Figure 16a shows that undoped PMMA-PVA nanocomposites exhibit an amorphous nature with a smooth surface. Figure 16 (b–e) shows the SEM images of ZnO NPs homogeneously spread on the surface of PMMA-PVA thin film matrix. The measured size of ZnO NPs lies in the (100–500) nm range in diameter. Obviously, good dispersion of ZnO NPs within the PMMA-PVA matrix is confirmed. Having obtained well-dispersed

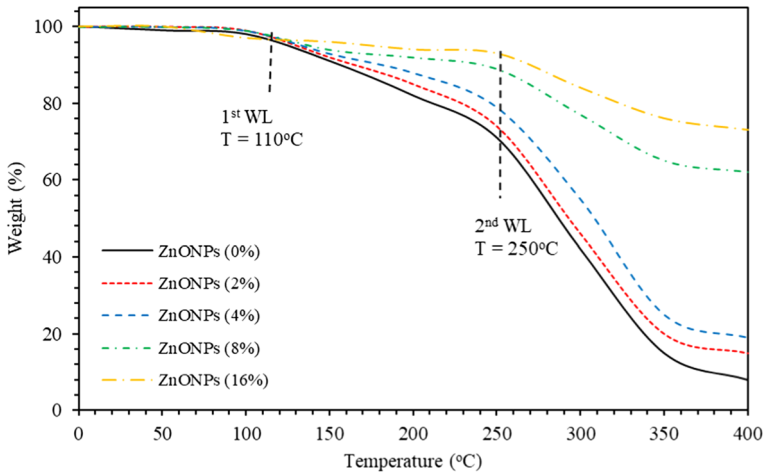


Fig. 15 The TGA curves of (PMMA-PVA)/ZnO NPs nanocomposites at different concentrations of ZnO NPs with respect to (PMMA-PVA) content

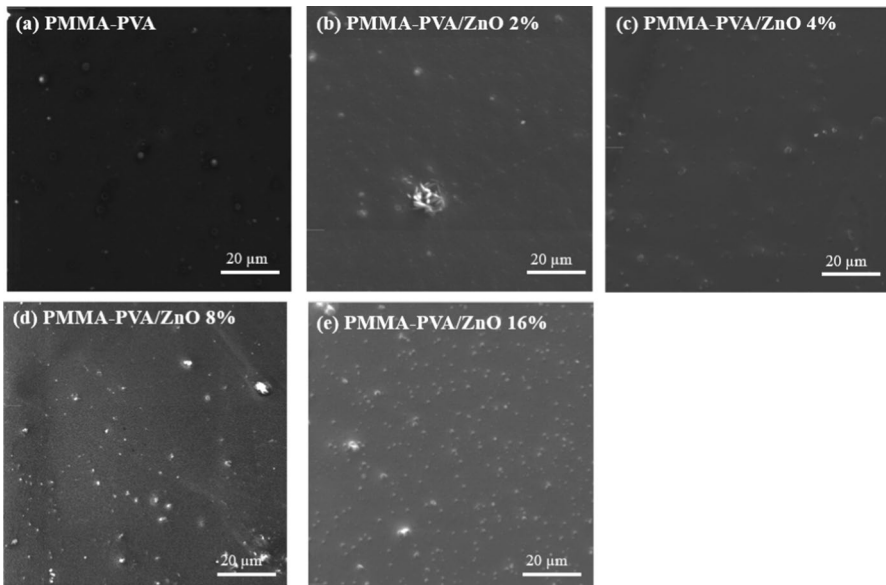


Fig. 16 The SEM micrographs of (PMMA-PVA)/ZnO NPs nanocomposite thin films at different concentrations of ZnO NPs

(PMMA-PVA)-ZnO NPs nanocomposites with four different ZnO NPs concentrations, we proceed with synthesis process of ZnO NPs for optical, chemical and thermal characterizations.

Conclusion

In summary, we report our results on synthesized (PMMA-PVA)/ZnO NPs nanocomposite thin films prepared using the dip coating technique. (PMMA-PVA)/ZnO NPs thin films are prepared using the (PMMA-PVA) polymeric solution added to wt% of (2%, 4%, 8%, and 16%) of (ZnO) NPs. The optical properties of the synthesized thin films are measured, characterized, and interpreted. In particular, transmittance, reflectance, refractive index, extinction coefficient, absorption coefficient, and the optical band-gap energy of synthesized thin films are measured and characterized. Furthermore, Urbach energy and dielectric functions are correlated with the UV–Vis measurements and calculated accordingly. On average, the transmittance of the undoped PMMA-PVA thin film is found to be 91.6% in the visible region. Our results indicate that transmittance of (PMMA-PVA)/ZnO NPs nanocomposite thin films gradually decrease upon incorporating (ZnO) nanoparticles in the polymeric matrix. Consequently, other relevant optical properties of doped polymeric thin films are affected accordingly.

In addition, the refractive index of undoped PMMA-PVA thin film is found to be in the range (1.48 and 1.72). Our results indicate that the refractive index of doped polymeric thin films increases as (ZnO) NPs content inserted in thin films is increased. Moreover, the optical band gap of undoped PMMA-PVA thin film is found to be 4.069 eV as extracted from the Tauc plot. Interestingly, optical band-gap energy of (PMMA-PVA)/ZnO NPs thin films are found to decrease (4.041 eV, 4.016 eV, 3.98 eV, and 3.96 eV) as (ZnO) NPs concentration incorporated in polymeric thin films is increased.

To obtain a deeper insight into the vibration modes of both polymeric thin-film system, FTIR absorbance spectra of (PMMA-PVA)/ZnO NPs nanocomposite thin film with different concentrations of (ZnO) NPs are measured in the spectral range of 500 cm^{-1} up to 4000 cm^{-1} . The FTIR profiles of (PMMA-PVA)-ZnO NPs nanocomposite thin films are found to exhibit vibrational bands at 1150.7 cm^{-1} that could be correlated with Zn–O bond. The observed increased bond intensity at 1725.08 cm^{-1} seems to be due to the stretching of the ester bond of PMMA-PVA. The variations of the peak's intensities of the whole FTIR spectra of (PMMA-PVA)/ZnO NPs nanocomposite thin films may be interpreted in terms of the intermolecular bonding between the PMMA-PVA nanocomposites and (ZnO) NPs.

The thermal stability of (PMMA-PVA)/ZnO NPs nanocomposite thin films is investigated using thermogravimetric analysis (TGA) at temperatures up to $400\text{ }^{\circ}\text{C}$. We found that the TGA profile of (PMMA-PVA)/ZnO NPs nanocomposite thin films exhibits two WL steps at 110 and $250\text{ }^{\circ}\text{C}$ irrespective of the degree of the merger of (ZnO) NPs into (PMMA-PVA) thin films. The WL of the nanocomposite thin films is inversely proportional to the wt% of (ZnO) NPs, confirming that physicochemical bonding density is strengthened upon increasing the incorporation degree of (ZnO) NPs into polymeric thin films. Advantageously, (PMMA-PVA)/ZnO NPs nanocomposite thin films are found to be thermally stable at temperatures below $110\text{ }^{\circ}\text{C}$ at which most of the optical applications can be

performed in spite of the slight and negligible slope in TGA curve below 110 °C which is mostly due to water/solvent adsorption that can be tackled appropriately.

Acknowledgements The authors would like to thank Jordan University of Science and Technology in Jordan for the support provided by the Deanship of Scientific Research on project No. 20180246 (Grant number: 282-2019). The authors would like to thank Prof. Borhan Albiss and Prof. M-Ali Al-Akhras for their help in using the facilities of the Center of Nanotechnology and the Lab. of Biomedical Physics.

Authors contribution AMA, ARAD, and AAA were involved in the data curation, methodology, data acquisition, writing—original draft preparation, and software. ASAI-A was involved in the data curation, methodology, writing, reviewing and editing. QMAI-B was involved in the investigation, data acquisition and analysis, conceptualization, methodology, and supervision.

Declaration

Conflict of interest The authors declare that they have no known competing financial interests or personal relationships that could have appeared to influence the work reported in this paper.

References

1. Fan X, Lin L, Messersmith PB (2006) Surface-initiated polymerization from TiO₂ nanoparticle surfaces through a biomimetic initiator: a new route toward polymer–matrix nanocomposites. *Compos Sci Technol* 66:1198–1204
2. Kuo M, Tsai C, Huang J, Chen M (2005) PEEK composites reinforced by nano-sized SiO₂ and Al₂O₃ particulates. *Mater Chem Phys* 90:185–195
3. Hammani S, Barhoum A, Bechelany M (2018) Fabrication of PMMA/ZnO nanocomposite: effect of high nanoparticles loading on the optical and thermal properties. *J Mater Sci* 53:1911–1921
4. Khoshnevisan K, Maleki H, Samadian H, Shahsavari S, Sarrafzadeh MH, Larijani B et al (2018) Cellulose acetate electrospun nanofibers for drug delivery systems: applications and recent advances. *Carbohydr Polym* 198:131–141
5. Naskar AK, Keum JK, Boeman RG (2016) Polymer matrix nanocomposites for automotive structural components. *Nat Nanotechnol* 11:1026
6. Yang Y, Dan Y (2003) Preparation of PMMA/SiO₂ composite particles via emulsion polymerization. *Colloid Polym Sci* 281:794–799
7. Chen M, Wu L, Zhou S, You B (2004) Synthesis of raspberry-like PMMA/SiO₂ nanocomposite particles via a surfactant-free method. *Macromolecules* 37:9613–9619
8. Xu P, Wang H, Tong R, Du Q, Zhong W (2006) Preparation and morphology of SiO₂/PMMA nanohybrids by microemulsion polymerization. *Colloid Polym Sci* 284:755–762
9. Hong R, Fu H, Zhang Y, Liu L, Wang J, Li H et al (2007) Surface-modified silica nanoparticles for reinforcement of PMMA. *J Appl Polym Sci* 105:2176–2184
10. Yeh J-M, Weng C-J, Liao W-J, Mau Y-W (2006) Anticorrosively enhanced PMMA–SiO₂ hybrid coatings prepared from the sol–gel approach with MSMA as the coupling agent. *Surface Coatings Technol* 201:1788–1795
11. M. Ohring, *Materials science of thin films*. Academic press, 2001.
12. A. Al.Sanableh, "structural and Optical Properties of ZnO Thin Films Deposited by Sol Gel Coating Technique," Manter Degree, Physics Department, Jordan University of Science and Technology Irbid, 2006.
13. Kim SS, Park TS, Shin BC, Kim YB (2005) Polymethyl methacrylate/montmorillonite nanocomposite beads through a suspension polymerization-derived process. *J Appl Polym Sci* 97:2340–2349
14. Yeum J-H, Deng Y (2005) Synthesis of high molecular weight poly (methyl methacrylate) microspheres by suspension polymerization in the presence of silver nanoparticles. *Colloid Polym Sci* 283:1172–1179
15. Otanicar TP, DeJarnette D, Hewakuruppu Y, Taylor RA (2016) Filtering light with nanoparticles: a review of optically selective particles and applications. *Adv Opt Photon* 8:541–585

16. Zheng J, Zhu R, He Z, Cheng G, Wang H, Yao K (2010) Synthesis and characterization of PMMA/SiO₂ nanocomposites by in situ suspension polymerization. *J Appl Polym Sci* 115:1975–1981
17. Mohammed M (2018) Optical properties of ZnO nanoparticles dispersed in PMMA/PVDF blend. *J Mol Struct* 1169:9–17
18. T. Siddaiah, P. Ojha, N. O. Kumar, and C. Ramu, "Structural, optical and thermal characterizations of PVA/MAA: EA polyblend films," *Mater Res* vol. 21, 2018.
19. Menazea A, Mostafa AM, Al-Ashkar EA (2020) Effect of nanostructured metal oxides (CdO, Al₂O₃, Cu₂O) embedded in PVA via Nd: YAG pulsed laser ablation on their optical and structural properties. *J Mol Struct* 1203:127374
20. Mansour A, Mansour S, Abdo M (2015) Improvement structural and optical properties of ZnO/PVA nanocomposites. *IOSR J Appl Phys* 7:60–69
21. Hemalatha K, Rukmani K, Suriyamurthy N, Nagabhushana B (2014) Synthesis, characterization and optical properties of hybrid PVA–ZnO nanocomposite: a composition dependent study. *Mater Res Bull* 51:438–446
22. Ghosh S, Srivastava P, Pandey B, Saurav M, Bharadwaj P, Avasthi D et al (2008) Study of ZnO and Ni-doped ZnO synthesized by atom beam sputtering technique. *Appl Phys A* 90:765–769
23. Das BK, Das T, Parashar K, Parashar S, Kumar R, Choudhary HK et al (2019) Investigation of structural, morphological and NTCR behaviour of Cu-doped ZnO nanoceramics synthesized by high energy ball milling. *Mater Chem Phys* 221:419–429
24. Das T, Das BK, Parashar K, Parashar S (2018) Modulus Spectroscopy and ac Conductivity of Zn_{1-x}CaxO Ceramics. *Adv Sci Lett* 24:5703–5707
25. Karpina V, Lazorenko V, Lashkarev C, Dobrowolski V, Kopylova L, Baturin V et al (2004) Zinc oxide–analogue of GaN with new perspective possibilities. *Cryst Res Technol J Exp Ind Crystallogr* 39:980–992
26. Hassan N, Hashim M, Al-Douri Y, Al-Heusein K (2012) Current dependence growth of ZnO nanostructures by electrochemical deposition technique. *Int J Electrochem Sci* 7:4625–4635
27. Al-Douri Y, Reshak AH, Ahmed WK, Ghazai AJ (2014) Structural and optical investigations of In doped ZnO binary compound. *Mater Express* 4:159–164
28. Al-Douri Y, Haider A, Reshak A, Bouhemadou A, Ameri M (2016) Structural investigations through cobalt effect on ZnO nanostructures. *Optik* 127:10102–10107
29. Al-Bataineh QM, Alsaad A, Ahmad A, Al-Sawalmih A (2019) Structural, Electronic and Optical Characterization of ZnO Thin Film-Seeded Platforms for ZnO Nanostructures: Sol-Gel Method Versus Ab Initio Calculations. *J Electron Mater* 48:5028–5038
30. Wang Z-S, Huang C-H, Huang Y-Y, Hou Y-J, Xie P-H, Zhang B-W et al (2001) A highly efficient solar cell made from a dye-modified ZnO-covered TiO₂ nanoporous electrode. *Chem Mater* 13:678–682
31. Lin H-M, Tzeng S-J, Hsiu P-J, Tsai W-L (1998) Electrode effects on gas sensing properties of nanocrystalline zinc oxide. *Nanostruct Mater* 10:465–477
32. Xu J, Pan Q, Tian Z (2000) Grain size control and gas sensing properties of ZnO gas sensor. *Sens Actuators B Chem* 66:277–279
33. Curri M, Comparelli R, Cozzoli P, Mascolo G, Agostiano A (2003) Colloidal oxide nanoparticles for the photocatalytic degradation of organic dye. *Mater Sci Eng C* 23:285–289
34. Kamat PV, Huehn R, Nicolaescu R (2002) A "sense and shoot" approach for photocatalytic degradation of organic contaminants in water. *J Phys Chem B* 106:788–794
35. Seung BP, Yun CK (1997) Photocatalytic activity of nanometer size ZnO particles prepared by spray pyrolysis. *J Aerosol Sci* 1001:S473–S474
36. Feldmann C (2003) Polyol-mediated synthesis of nanoscale functional materials. *Adv Funct Mater* 13:101–107
37. Zheng M, Zhang L, Li G, Shen W (2002) Fabrication and optical properties of large-scale uniform zinc oxide nanowire arrays by one-step electrochemical deposition technique. *Chem Phys Lett* 363:123–128
38. Wu R, Xie C (2004) Formation of tetrapod ZnO nanowhiskers and its optical properties. *Mater Res Bull* 39:637–645
39. Kitano M, Shiojiri M (1997) Benard convection ZnO/resin lacquer coating—a new approach to electrostatic dissipative coating. *Powder Technol* 93:267–273
40. Kim JH, Choi WC, Kim HY, Kang Y, Park Y-K (2005) Preparation of mono-dispersed mixed metal oxide micro hollow spheres by homogeneous precipitation in a micro precipitator. *Powder Technol* 153:166–175

41. Damonte L, Zélis LM, Soucase BM, Fenollosa MH (2004) Nanoparticles of ZnO obtained by mechanical milling. *Powder Technol* 148:15–19
42. Zhao X, Zheng B, Li C, Gu H (1998) Acetate-derived ZnO ultrafine particles synthesized by spray pyrolysis. *Powder Technol* 100:20–23
43. Hong R, Xu L, Ren Z, Lin X, Li H (2005) Nanosized zinc oxide prepared by homogeneous precipitation and its photocatalytic property. *Environ Prot Chem Ind* 23:231–234
44. Alsaad A, Bataineh QM, Ahmad A, yousef Jum'h I, Alaqtash N, Bani-Salameh A (2020) Optical properties of transparent PMMA-PS/ZnO NPs polymeric nanocomposite films: UV-Shielding applications. *Mater Res Express*
45. Hajibeygi M, Maleki M, Shabaniyan M, Ducos F, Vahabi H (2018) New polyvinyl chloride (PVC) nanocomposite consisting of aromatic polyamide and chitosan modified ZnO nanoparticles with enhanced thermal stability, low heat release rate and improved mechanical properties. *Appl Surf Sci* 439:1163–1179
46. Alami ZY, Salem M, Gaidi M (2018) Structural, optical and electrical characterizations of ZnO/PS. In: MATEC web of conferences, 2018, p 00013
47. Hemalatha K, Rukmani K (2017) Concentration dependent dielectric, AC conductivity and sensing study of ZnO-polyvinyl alcohol nanocomposite films. *Int J Nanotechnol* 14:961–974
48. Ahmad A, Alsaad A, Al-Bataineh Q, Al-Naafa M (2018) Optical and structural investigations of dip-synthesized boron-doped ZnO-seeded platforms for ZnO nanostructures. *Appl Phys A* 124:458
49. Kittel C (1986) Introduction to solid state physics, 6th edn., translated by Y, Uno, N. Tsuya, A. Morita and J. Yamashita, (Maruzen, Tokyo, 1986) pp, pp 124–129
50. Jin ZC, Hamberg I, Granqvist C (1988) Optical properties of sputter-deposited ZnO: Al thin films. *J Appl Phys* 64:5117–5131
51. Mir FA (2014) Transparent wide band gap crystals follow indirect allowed transition and bipolaron hopping mechanism. *Results Phys* 4:103–104
52. Fasasi A, Osagie E, Pelemo D, Obiajunwa E, Ajenifuja E, Ajao J et al (2018) Effect of precursor solvents on the optical properties of copper oxide thin films deposited using spray pyrolysis for optoelectronic applications. *Am J Mater Synth Process* 3:12–22
53. Spitzer W, Fan H (1957) Determination of optical constants and carrier effective mass of semiconductors. *Phys Rev* 106:882
54. Hassanien AS (2016) Studies on dielectric properties, opto-electrical parameters and electronic polarizability of thermally evaporated amorphous Cd50S50– xSex thin films. *J Alloy Compd* 671:566–578
55. Farag A, Ashery A, Shenashen M (2012) Optical absorption and spectrophotometric studies on the optical constants and dielectric of poly (o-toluidine)(POT) films grown by spin coating deposition. *Phys B* 407:2404–2411
56. Ibupoto Z, Khun K, Beni V, Liu X, Willander M (2013) Synthesis of novel CuO nanosheets and their non-enzymatic glucose sensing applications. *Sensors* 13:7926–7938
57. Sun F, Hung H-C, Sinclair A, Zhang P, Bai T, Galvan DD et al (2016) Hierarchical zwitterionic modification of a SERS substrate enables real-time drug monitoring in blood plasma. *Nat Commun* 7:1–9
58. Huang CL, Steele TW, Widjaja E, Boey FY, Venkatraman SS, Loo JS (2013) The influence of additives in modulating drug delivery and degradation of PLGA thin films. *NPG Asia Mater* 5:e54–e54
59. Harrison RH, Steele JA, Chapman R, Gormley AJ, Chow LW, Mahat MM et al (2015) Modular and versatile spatial functionalization of tissue engineering scaffolds through fiber-initiated controlled radical polymerization. *Adv Funct Mater* 25:5748–5757
60. Green MA (2007) Thin-film solar cells: review of materials, technologies and commercial status. *J Mater Sci Mater Electron* 18:15–19
61. Lin J, Guo J, Liu C, Guo H (2016) Ultrahigh-performance Cu₂ZnSnS₄ thin film and its application in microscale thin-film lithium-ion battery: comparison with SnO₂. *ACS Appl Mater Interfaces* 8:34372–34378
62. Ross CA, Berggren KK, Cheng JY, Jung YS, Chang JB (2014) Three-dimensional nanofabrication by block copolymer self-assembly. *Adv Mater* 26:4386–4396
63. Hashizume M, Murata Y, Iijima K, Shibata T (2016) Drug loading and release behaviors of free-standing polysaccharide composite films. *Polym J* 48:545–550
64. Rahman A (2013) Medico-ethnobotany: a study on the tribal people of Rajshahi Division, Bangladesh. *Peak J Med Plants Res* 1:1–8

65. Kim JH, Jang J, Zin W-C (2001) Thickness dependence of the glass transition temperature in thin polymer films. *Langmuir* 17:2703–2710
66. Fedorchenko AI, Wang A-B, Cheng HH (2009) Thickness dependence of nanofilm elastic modulus. *Appl Phys Lett* 94:152111
67. Michell RM, Blaszczyk-Lezak I, Mijangos C, Müller AJ (2013) Confinement effects on polymer crystallization: from droplets to alumina nanopores. *Polymer* 54:4059–4077
68. Laroche G, Fitremann J, Gherardi N (2013) FTIR-ATR spectroscopy in thin film studies: the importance of sampling depth and deposition substrate. *Appl Surf Sci* 273:632–637
69. Wang Y, Ge S, Rafailovich M, Sokolov J, Zou Y, Ade H (2004) ning, JL; Lustiger, A.; Maron, G. *Macromolecules* 37:3319
70. Ohta K, Iwamoto R (1985) Experimental proof of the relation between thickness of the probed surface layer and absorbance in FT-IR/ATR spectroscopy. *Appl Spectrosc* 39:418–425
71. Ramin MA, Le Bourdon G, Daugey N, Bennetau B, Vellutini L, Buffeteau T (2011) PM-IRRAS investigation of self-assembled monolayers grafted onto SiO₂/Au substrates. *Langmuir* 27:6076–6084
72. Baibarac M, Cochet M, Łapkowski M, Mihut L, Lefrant S, Baltog I (1998) SERS spectra of polyaniline thin films deposited on rough Ag, Au and Cu. Polymer film thickness and roughness parameter dependence of SERS spectra. *Synth Met* 96:63–70
73. Kim J, Cho J, Seidler PM, Kurland NE, Yadavalli VK (2010) Investigations of chemical modifications of amino-terminated organic films on silicon substrates and controlled protein immobilization. *Langmuir* 26:2599–2608
74. Song S, Chu R, Zhou J, Yang S, Zhang J (2008) Formation and tribology study of amide-containing stratified self-assembled monolayers: influences of the underlayer structure. *J Phys Chem C* 112:3805–3810
75. Haider Mohammed Shanshool MY, Wan Mahmood Mat Yunus, bIbtisamYahya (2015) Abdullah Optical properties of PMMA/ZnO Nanocomposites as foils prepared by casting method. *Aust J Basic Appl Sci*

Publisher's Note Springer Nature remains neutral with regard to jurisdictional claims in published maps and institutional affiliations.

Authors and Affiliations

A. M. Alsaad¹  · Abdul Raouf Al Dairy² · A. A. Ahmad¹ · Ayah S. Al-anbar² · Qais M. Al-Bataineh¹

¹ Department of Physical Sciences, Jordan University of Science & Technology, P.O. Box 3030, Irbid 22110, Jordan

² Department of Physics, Yarmouk University, Irbid 21163, Jordan